Basin-scale estimates of pelagic and coral reef calcification in the Red Sea and Western Indian Ocean

Zvi Steiner[a,b], Jonathan Erez[a,b], Aldo Shemesh[c], Ruth Yam[c], Amitai Katz[a], and Boaz Lazar[a,b,1]

[a]The Fredy and Nadine Herrmann Institute of Earth Sciences, The Hebrew University, Jerusalem 91904, Israel; [b]The Interuniversity Institute for Marine Sciences, Eilat 88103, Israel; and [c]Department of Earth and Planetary Sciences, Weizmann Institute of Science, Rehovot 76100, Israel

Edited by Mark H. Thiemens, University of California, San Diego, La Jolla, CA, and approved September 30, 2014 (received for review July 28, 2014)

Basin-scale calcification rates are highly important in assessments of the global oceanic carbon cycle. Traditionally, such estimates were based on rates of sedimentation measured with sediment traps or in deep sea cores. Here we estimated $CaCO_3$ precipitation rates in the surface water of the Red Sea from total alkalinity depletion along their axial flow using the water flux in the straits of Bab el Mandeb. The relative contribution of coral reefs and open sea plankton were calculated by fitting a Rayleigh distillation model to the increase in the strontium to calcium ratio. We estimate the net amount of $CaCO_3$ precipitated in the Red Sea to be $7.3 \pm 0.4 \cdot 10^{10}$ kg·y^{-1} of which 80 ± 5% is by pelagic calcareous plankton and 20 ± 5% is by the flourishing coastal coral reefs. This estimate for pelagic calcification rate is up to 40% higher than published sedimentary $CaCO_3$ accumulation rates for the region. The calcification rate of the Gulf of Aden was estimated by the Rayleigh model to be ∼1/2 of the Red Sea, and in the northwestern Indian Ocean, it was smaller than our detection limit. The results of this study suggest that variations of major ions on a basin scale may potentially help in assessing long-term effects of ocean acidification on carbonate deposition by marine organisms.

$CaCO_3$ precipitation | alkalinity | Sr/Ca | Rayleigh distillation | Red Sea

The anthropogenic CO_2 accumulating rapidly in the atmosphere acidifies the ocean surface waters at an increasing rate (1). Ocean acidification lowers the saturation state of $CaCO_3$ minerals, making it harder for calcifying organisms to build their skeletons (2). The actual effect of ocean acidification on biogenic $CaCO_3$ precipitation rates is highly variable and species specific (3). Since this issue is of considerable importance to the functioning of many marine ecosystems, it has been intensively studied during recent years (4, 5). Most field studies are, however, site specific, conducted separately on marginal and pelagic environments. Here we provide a basin-scale (the whole Red Sea) approach to assess simultaneously the overall calcification rates of coral reefs and pelagic plankton communities using nonconservative geochemical trends.

The Red Sea (RS) is a long (∼2,250 km) and narrow (maximum width ∼350 km) embryonic ocean basin extending from 12.5°N to 30°N (Fig. 1). It is connected to the Gulf of Aden (GoAd) and the Indian Ocean (IO) by the shallow and narrow straits of Bab el Mandeb (BeM) (6). The excess evaporation (over precipitation) is ∼2 m·y^{-1} (7), and the absence of any significant river entering the RS drives a northward thermohaline flow of surface water from the GoAd into the RS against the prevailing northern winds during winter (8). A series of mesoscale eddies along the RS (9) increases the horizontal mixing. During June–September, the northeast monsoon is reversed toward southwest over the IO, inverting the direction of surface water flow in the northern IO, GoAd, and southern RS. The flow reversal induces intense upwelling and very high productivity along the western coasts of these regions (10). Surface water flow in the central and northern RS maintains its south-to-north direction throughout the year (11).

Average water exchange between the RS and GoAd through the straits of BeM is 0.4 Sv (1 Sv = 10^6 m^3·s^{-1}) (6). The shallow sill (137 m deep) at the straits separates between the deep water of the two basins. RS deepwater forms in the northern Red Sea (NRS), in complete isolation from oceanic deep water (12), as shown by the general circulation scheme (Fig. 1*B*). This setting leads to a unique phenomenon, homogenous bottom water temperature of above 21 °C (13), which maintains calcite and aragonite oversaturation at all depths (14). The warm surface water temperature in the RS is an important factor for the flourishing coral reefs that fringe much of its coasts (Fig. 1). In the NRS, the coral reefs band is almost continuous along its coasts, while further south, coral reefs extend offshore due to the wide and shallow shelf (15). The estimated total reef area in the RS is ∼$17 \cdot 10^3$ km^2 (16). In the GoAd, strong wave energy and upwelling of high-nutrient water limit coral habitat to 5% of the Yemenite coast (15). The calcareous plankton population in the pelagic RS and western IO comprises coccolithophores, planktonic foraminifera, and pteropods in varying proportions (17, 18).

The clear south–north salinity gradient along the RS (refs. 8 and 13 and Fig. 1*C*) is expected to produce a relative increase in the concentrations of all conservative dissolved ions. The concentrations of the major elements, Ca, Sr, Mg, and total alkalinity (A_T), however, may deviate from this conservative behavior (as do many trace elements) because they coprecipitate with biogenic $CaCO_3$ formed by either pelagic calcareous plankton or coral reefs on the margins. The deviation of Ca and A_T from conservative behavior depends on the amount of $CaCO_3$ deposited. The deviation of Sr and Mg depends also on their partitioning into the major $CaCO_3$ minerals, calcite and aragonite. The Sr/Ca and Mg/Ca ratios along the RS should therefore vary according to their distribution coefficients in the

Significance

This approach of estimating basin-scale calcification rates and the relative role of margins (reefs) versus pelagic carbonate deposition can be applied as a long-term monitoring scheme for the effects of ocean acidification. The database for the response of individual organisms to elevated CO_2 levels is growing steadily, but in situ measurements assessing this response are very local. The study demonstrates the feasibility of estimating the relative calcification rates of planktonic and benthic populations over a whole basin and provides a tool for the monitoring of these complex systems on large spatial scales.

Author contributions: J.E. and B.L. designed research; A.S., R.Y., A.K., and B.L. performed research; Z.S., J.E., A.K., and B.L. analyzed data; and Z.S., J.E., and B.L. wrote the paper.

The authors declare no conflict of interest.

This article is a PNAS Direct Submission.

Freely available online through the PNAS open access option.

[1]To whom correspondence should be addressed. Email: boaz.lazar@mail.huji.ac.il.

This article contains supporting information online at www.pnas.org/lookup/suppl/doi:10.1073/pnas.1414323111/-/DCSupplemental.

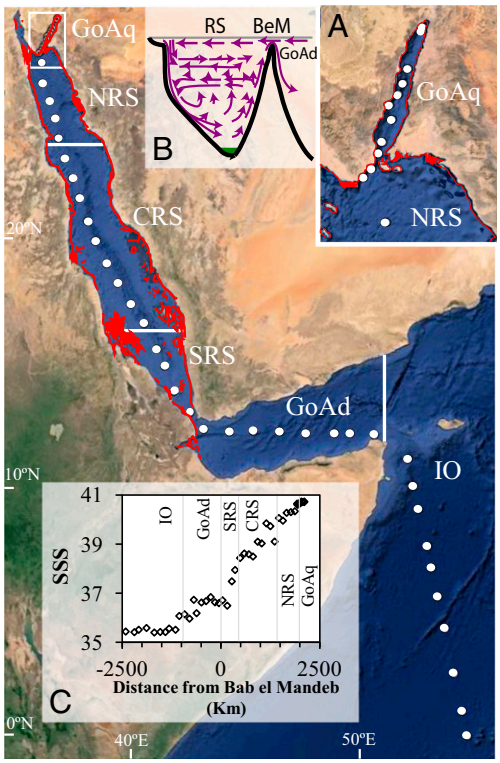

Fig. 1. Location map of the sampling stations (white dots) presented on a Google Earth image. (*A*) A zoom-in to the Gulf of Aqaba. (*B*) A scheme of the general circulation in the Red Sea (RS). Modified with permission from ref. 12. Arrows represent the main flow patterns, and the green area at the bottom of RS illustrates the hot brines. BeM, Bab el Mandeb. (*C*) A plot of sea surface salinity (SSS) versus the northward distance from BeM toward the RS. The coral reefs along the RS are drawn in red using the map in ref. 56. The white solid lines in the main image are the borders between the different geographical regions as defined in this study: CRS, Central Red Sea (16°N–23.5°N); GoAd, Gulf of Aden; GoAq, Gulf of Aqaba; IO, Indian Ocean; NRS, North Red Sea (Straits of Tiran to 23.5°N); SRS, South Red Sea (Bab el Mandeb to 16°N).

precipitated mineral phases. The distribution coefficient of either Sr or Mg in $CaCO_3$, K_D, is defined as:

$$K_D = \frac{\frac{m_M^S}{m_{Ca^{2+}}^S}}{\frac{m_M^{sw}}{m_{Ca^{2+}}^{sw}}}, \quad [1]$$

where m denotes the concentration of the metal ion, the subscript M denotes either Sr^{2+} or Mg^{2+}, and the superscripts S and sw denote the solid phase ($CaCO_3$, either aragonite or calcite) and seawater, respectively.

According to Eq. **1**, when seawater flow unidirectional within an enclosed basin while $CaCO_3$ is continuously precipitated, then, if $K_D = 1$, the ratio $m_M^{sw}/m_{Ca^{2+}}^{sw}$ will not change; if $K_D < 1$, the ratio $m_M^{sw}/m_{Ca^{2+}}^{sw}$ will increase; and if $K_D > 1$, the ratio $m_M^{sw}/m_{Ca^{2+}}^{sw}$ will decrease.

Results and Discussion

Nonconservative Trends Along the Red Sea Transect. Details of IO to RS sampling locations and water analyses are provided in Table S1. As indicated above, due to excess evaporation over precipitation in the RS, surface seawater salinity (SSS) increases northward (Fig. 1*C*). The SSS trend is accompanied by a conservative increase northward in the concentrations of part of the major ions and nonconservative decrease in others (Table S1). Specifically A_T, Ca, Sr, and Mg show a clear northward decrease when normalized to constant salinity according to the equation: $C_N = 35 \cdot C_M/\text{salinity}$, where C_N is the normalized concentration and C_M is the measured concentration (Table 1). For example, the clear increase in A_T when plotted versus salinity (Fig. 2*A*) translates to a northward decrease when A_T is normalized to a constant salinity (Fig. 2*B*). Recalculation of earlier A_T data collected in the RS (13, 14, 19, 20) shows that the normalized A_T below the pycnocline is constant and lower than the surface values.

Average $CaCO_3$ precipitation (G) within the RS was calculated by $G = \rho \cdot F \cdot \Delta A_T$, where ρ is the average seawater density (1,025 $kg \cdot m^{-3}$), F is the water flux through BeM [0.4 Sv (6)], and ΔA_T is the difference between the A_T of western GoAd (station SY35 in Table S1) and average Gulf of Aqaba (GoAq). This calculation assumed that RS surface water is losing alkalinity due to $CaCO_3$ deposition during its "journey" northward within the RS. The equation above yields a $CaCO_3$ precipitation rate for the RS of $1.45 \pm 0.07 \cdot 10^{12}$ $eq \cdot y^{-1}$. It is reassuring that this calcification rate falls right between two earlier estimates, $1.65 \cdot 10^{12}$ $eq \cdot y^{-1}$ based on fluxes in the Strait of BeM (21) and $1.2 \cdot 10^{12}$ $eq \cdot y^{-1}$ based on a RS box model (13). This estimate is probably affected by vertical mixing of surface water with A_T depleted intermediate water. The maximum effect of this vertical mixing on the calcification rate estimate is in the range of 5–15% as calculated from residence time of water in the RS and diapycnal mixing (see *SI Text* for citation and explanation).

Long-Term Steady State of the System. The isotopic composition of seawater hydrogen and oxygen reflects the balance between water evaporation, precipitation, and water–rock interactions. Measured δD versus $\delta^{18}O$ slope for the RS and GoAd in November 1998 was 6.0 (Fig. S1), identical to the slope measured by Craig during the early 1960s (22). The constancy of the RS δD–$\delta^{18}O$ slope over a time interval similar to the residence time of water in the RS (12, 23) suggests that over this period, the water balance in the RS was fairly constant. This is corroborated by the long-term similarity (within analytical error) of normalized A_T data collected by the expeditions of GEOSECS 1977 (20), Merou II 1982 (13), and the present study (Fig. 2*B*). Constancy in $CaCO_3$

Table 1. Averaged concentrations of the alkaline earth metals, A_T, and water isotopic composition for all regions considered in this study

Region	Mg^{2+} $meq \cdot kg^{-1}$	Ca^{2+} $meq \cdot kg^{-1}$	Sr^{2+} $\mu eq \cdot kg^{-1}$	A_T $\mu eq \cdot kg^{-1}$	$\delta^{18}O$ ‰	δD ‰
Gulf of Aqaba	103.6 ± 0.2	20.2 ± 0.2	167.6 ± 0.6	2141 ± 1	2.03 ± 0.10	12.3 ± 0.6
Northern Red Sea	103.5 ± 0.1	20.3 ± 0.3	167.9 ± 0.8	2147 ± 5	1.95 ± 0.11	11.4 ± 0.7
Central Red Sea	103.8 ± 0.1	20.5 ± 0.3	168.5 ± 0.7	2174 ± 8	1.55 ± 0.10	9.8 ± 0.6
Southern Red Sea	104.1 ± 0.1	20.7 ± 0.2	170.2 ± 0.5	2234 ± 19	1.16 ± 0.12	6.8 ± 0.9
Gulf of Aden	104.0 ± 0.2	20.7 ± 0.3	169.7 ± 0.7	2272 ± 8	0.98 ± 0.11	5.7 ± 1.0
Western Indian Ocean	104.0 ± 0.2	20.8 ± 0.3	168.9 ± 0.8	2281 ± 5	0.76 ± 0.08	4.9 ± 0.8

Ionic concentrations and A_T were normalized to salinity of 35‰. The error bars represent the average deviations from the mean of all measurements in each region.

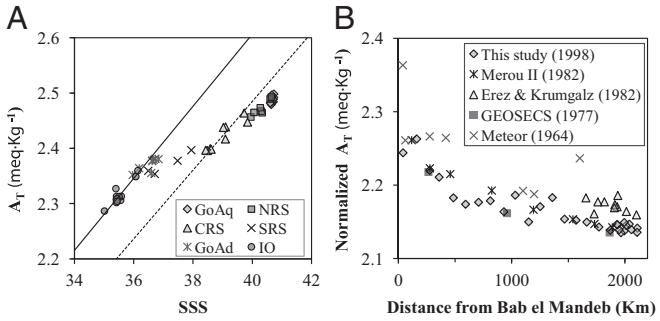

Fig. 2. Sea surface alkalinity (A_T) in all stations along the Indian Ocean–Red Sea (Fig. 1). (*A*) A_T versus SSS in all stations. The analytical errors are smaller than the symbol sizes. The markers denote the different geographical regions (Fig. 1). The straight lines represent the conservative trends (both lines starting from the origin) for average Indian Ocean (solid line) and average Central Red Sea (dashed line) A_T; points below the conservative lines represent $CaCO_3$ precipitation. (*B*) Surface water A_T normalized to mean ocean water salinity of 35 versus the northward distance from Bab el Mandeb as measured in the Red Sea during four earlier cruises and the present study (13, 14, 19, 20). The data show that A_T varied conservatively along the western Indian Ocean and started to deviate from conservative behavior at the Gulf of Aden. Within the Red Sea, the normalized A_T of the surface water decreased from south to north by 5%. A steep decrease in A_T was observed in the southern Red Sea, between latitudes 14°N and 16°N (150–500 km north of Bab el Mandeb) where coral reefs are abundant.

deposition rate between the 1940s and 1998 was previously demonstrated in a coral colony from the central Red Sea (CRS) (24).

The Contributions of Coral Reefs and Pelagic Plankton to Calcification on a Basin Scale. The ratio between the amounts of Sr and Ca removed from the water along the RS allows estimation of the relative contributions of the pelagic system and coral reefs to $CaCO_3$ production in the basin. The major three calcareous plankton communities have low K_D for Sr in their $CaCO_3$ skeletons: fresh pteropod tests have $K_D \approx 0.12$ (25), the average K_D for planktonic foraminifera is the same (26), and for coccolithophores, $K_D \approx 0.3$ (27–29). Recent sediments from intermediate depths at the CRS contain equal abundance of pteropods and planktonic foraminifers (17). Sediment trap data from the western Arabian Sea show that annual average mass accumulation ratio of planktonic foraminifera to coccolithophores is 1.24, with very high temporal variability (30). This flux ratio is compatible with the foraminifera/coccolithophore standing stock ratio of 5 in surface water along the RS, GoAd, and Arabian Sea (31) (note that the reproduction rate of coccolithophores is an order of magnitude faster than that of foraminifera and pteropods). Accordingly, the average distribution coefficient of Sr in calcareous plankton, K_D^{plankton}, is 0.17 ± 0.03 (assuming that coccolithophore comprise 10–40% of the total $CaCO_3$ flux of calcareous plankton in the RS and northwestern IO).

Aragonite corals have $K_D > 1$ for Sr, much higher than that of calcareous plankton. The Sr/Ca ratio in *Porites* coral skeletons is 9.04 ± 0.17 mmol·mol^{-1} at 25 °C, as calculated from 37 Sr/Ca versus temperature relations (32). Considering a global average Sr/Ca ratio in seawater of 8.52 mmol·mol^{-1} (33), this yields an average K_D of 1.06 ± 0.02 for coralline aragonite. A similar value of 1.04 ± 0.03 was measured in *Porites* corals from the GoAq (34) and was used here to represent the K_D of average reef, K_D^{reef}.

Precipitation of $CaCO_3$ is expected to change the Sr/Ca ratio of RS water during its northward travel according to the weighted (average) distribution coefficient of Sr in $CaCO_3$ precipitated by pelagic plankton and coral reefs as described by the classic Rayleigh distillation model (35):

$$\frac{R_w}{R_0} = f^{K_D - 1}, \qquad [2]$$

where K_D is the weighted distribution coefficient of Sr in biogenic (plankton + reef) $CaCO_3$, R_w is the Sr/Ca concentration ratio at a certain location within the region, R_0 is the Sr/Ca concentration ratio at the point of highest surface water Ca concentration, and f is the fraction of remaining normalized Ca ($f = [Ca]_w/[Ca]_0$). For nutrient poor waters, A_T decrease due to $CaCO_3$ precipitation can also be described by Eq. **2**.

A best fit to the RS data plotted in the form of Eq. **2** yields a power (K_D−1) of -0.65 for remaining Ca (Fig. 3*A*) or -0.66 for remaining A_T (Fig. S2) that translate to very similar overall K_D for Sr: 0.35 and 0.34 based on Ca and A_T, respectively. Assuming that all $CaCO_3$ within the RS is biogenic and formed by calcareous plankton and marginal reefs, their relative amounts can be estimated from the average K_D by the equation:

$$K_D = K_D^{\text{plankton}} \cdot X_{\text{plankton}} + K_D^{\text{reef}} \cdot (1 - X_{\text{plankton}}), \qquad [3]$$

where X_{plankton} is the proportion of $CaCO_3$ precipitated by pelagic plankton. Eq. **3** yields an $X_{\text{plankton}} = 0.80 \pm 0.05$, meaning that calcareous plankton produced ~80% of the $CaCO_3$ in the RS and coral reefs produced ~20%. Applying a Rayleigh distillation model is valid for the surface water of the RS because $CaCO_3$ precipitation proceeds while the water travels northward. The precipitated $CaCO_3$ sinks down and leaves the system and hence does not back-react with the seawater. The same approach was used to estimate the average K_D for Sr for the GoAd

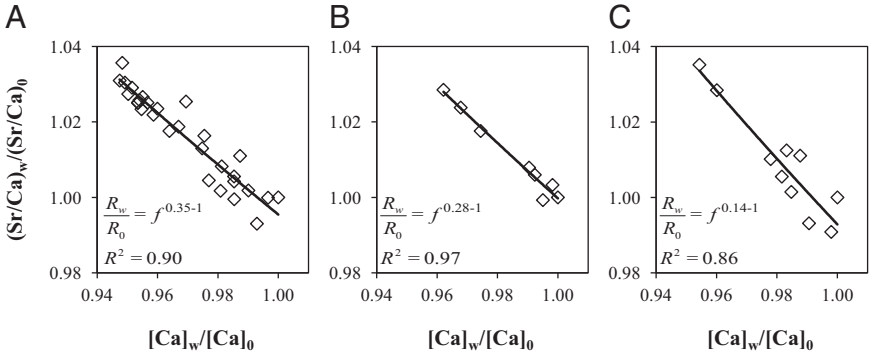

Fig. 3. Calculation of the average distribution coefficient (K_D) for strontium in $CaCO_3$ according to Eq. **2**. R_w is $(Sr/Ca)_w$, the concentration ratio at a certain location; R_0 is $(Sr/Ca)_0$, the concentration ratio at the point of highest Ca concentration for each region, and f is the fraction of remaining normalized Ca ($f = [Ca]_w/[Ca]_0$). The power of the line fit yielded the values of apparent K_D−1 of Sr for the regions: (*A*) Red Sea, (*B*) Gulf of Aden, and (*C*) Western Indian Ocean north of the equator.

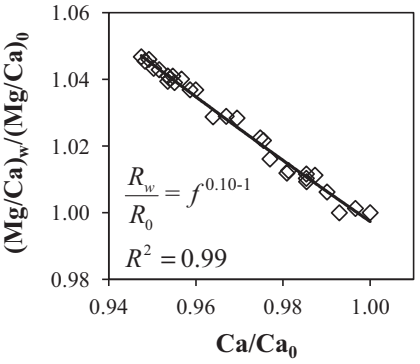

Fig. 4. Calculation of the Red Sea apparent K_D of Mg, using Eq. **2**. R_w, R_0, and f are the concentration ratios $(Mg/Ca)_w$ and $(Mg/Ca)_0$ and the fraction of remaining Ca, defined similarly to the definitions for the Sr/Ca ratios in Fig. 3; the power of the line fit yielded the value of apparent K_D−1 of Mg. Note that the calculation yields an apparent K_D of Mg of 0.10, which is approximately tenfold larger than K_D of Mg in either calcite or aragonite, suggesting that a process other the $CaCO_3$ precipitation is responsible for the Mg depletion in the Red Sea (see *The Contributions of Coral Reefs and Pelagic Plankton to Calcification on a Basin Scale*).

(K_D = 0.28, Fig. 3*B*) and northwestern IO (K_D = 0.14, Fig. 3*C*). Substituting these values into Eq. **3** yields X_{plankton} of 0.87 ± 0.07 for the GoAd and ∼1 for the northwest IO. This means that coral reefs precipitated 13 ± 7% of the $CaCO_3$ in the GoAd while their effect in the northwest IO is below the detection limit of this method. The value of the average K_D for the northwest IO suggests that foraminifera and pteropods are responsible for almost all $CaCO_3$ production (∼90%) in this region, while the role of coccolithophores (∼10%) is within the estimation error.

A similar calculation of the average Mg distribution coefficient in $CaCO_3$ using Eq. **2** provides another tool to distinguish between $CaCO_3$ precipitation by pelagic plankton and benthos. The highest biogenic K_D for Mg is 0.03, which is typical for calcite precipitated by echinoderms and a few other invertebrates (36). In foraminifera, benthic shallow species generally build their shells from high-Mg calcite with an average Mg K_D = 0.01 (37), while planktonic forms precipitate low-Mg calcite with an average K_D = 0.001 (38). Coral aragonite also contain very low Mg with an average K_D = 0.001 (39). In the RS, deep sea sediments contain significant amounts of high-Mg calcite with a nearly uniform Mg content of 12 mol % (K_D = 0.024) (40). All these K_D values for Mg are far lower than the apparent average K_D for Mg of 0.10 ± 0.02 calculated by fitting Eq. **2** for the entire RS (Fig. 4). This means that processes other than precipitation of calcite and aragonite may be responsible for the Mg decrease along the RS. A possible low-Mg source in the RS is the submarine hot brine "lakes" filling large portions of its deep basin (Fig. 1*B*) (41). These brines have extremely low Mg and may mix turbulently with the surface water to lower their Mg/Ca ratio. The effect of these brines on the RS Sr/Ca ratio (and hence on our estimate of the apparent Sr K_D) is negligible because their Sr/Ca ratio is much closer to that of RS deepwater (41). If the 0.5% Mg decrease observed in the RS resulted solely from mixing of hot brines, its total effect on decreasing RS Sr would amount to <4% of the observed Sr depletion. It is possible that the Mg deficiency we report in the RS was previously recorded as an Mg minimum at 800 m depth in the northwest Arabian Sea that was attributed to the influx of Mg-poor RS waters (42).

Red Sea Calcification Rates in a Global Context. The RS $CaCO_3$ precipitation rates as calculated above in $eq{\cdot}y^{-1}$ units translate to mass units of 7.3 ± 0.4·10^{10} $kg{\cdot}y^{-1}$, of which, pelagic plankton precipitated 5.8 ± 0.4·10^{10} $kg{\cdot}y^{-1}$ (80 ± 5%) and coral reefs precipitated 1.5 ± 0.4·10^{10} $kg{\cdot}y^{-1}$. Dividing the reef estimated rate by the total RS reefs area yields a $CaCO_3$ deposition flux in RS reefs of 0.9 $kg{\cdot}m^{-2}{\cdot}y^{-1}$. This rate is in excellent agreement with the average $CaCO_3$ deposition rate of a "complete reef system" of 1 $kg{\cdot}m^{-2}{\cdot}y^{-1}$ compiled by Kinsey (43) for different Pacific and Indian Ocean coral reefs.

A recent compilation of numerous alkalinity–salinity relationships for the global ocean reveals an outstanding, very low, alkalinity to salinity ratio for the western IO and RS, suggesting that this is a high $CaCO_3$ production oceanic region (44). The net RS pelagic $CaCO_3$ export production estimated in the current study is 1.35 ± 0.15 $mol{\cdot}m^{-2}{\cdot}y^{-1}$ (calcareous plankton calcification rate divided by the RS area of 440·10^3 km^2 minus the reef area). This value is more than tenfold the global average sedimentation rate at 2,000 m measured from sediment traps and threefold the oceanic maximum measured in the Arabian Sea (45) (Fig. 5). This high-alkalinity-based estimate of calcification rates relative to sediment traps suggests that either sediment traps collect material that has already undergone significant dissolution or that the high temperature and salinity of the RS induces extremely high calcification rates. Indeed, it was calculated that more than 60% of the exported $CaCO_3$ in the oceans dissolves between 200 m and 1,500 m (45, 46). The calculated dissolution rates in the IO were particularly high (46, 47), and, when added to the trap data, they close the gap between Arabian and Red Sea calcification rates.

The calcification rates calculated in this study are very similar to, yet slightly higher than, the sedimentary $CaCO_3$ accumulation rates from northern GoAq and SRS cores (Fig. 5). At the same time, they are about twice the $CaCO_3$ accumulation rates from northern and central RS cores. The latter cores were collected under deeper water column with slower sedimentation rates that may allow more time for $CaCO_3$ dissolution induced by oxygenic remineralization of organic matter (40, 48). The comparison with sedimentary $CaCO_3$ accumulation rates strongly supports that our calculated calcification rates represent export production of $CaCO_3$ and that lower accumulation rates at several sites represent dissolution. Another line of evidence to support dissolution in the RS is the observation that most of the pteropod

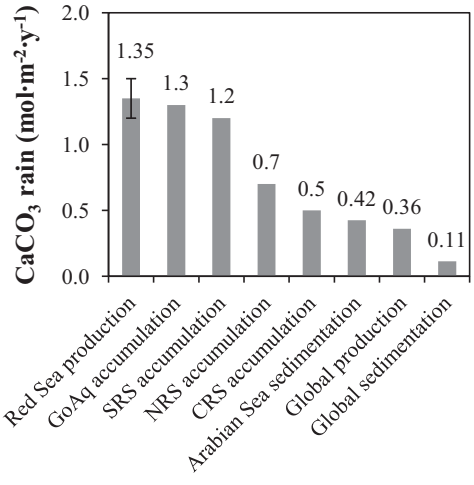

Fig. 5. Pelagic Red Sea $CaCO_3$ export production rate calculated in this study (left bar) compared with $CaCO_3$ accumulation rates calculated from literature data for sediments from four different RS regions: GoAq (54), SRS (18), NRS (54), and CRS (17); and for Arabian Sea $CaCO_3$ sedimentation (45) at 2,000 m, estimated global average $CaCO_3$ production (57) and average global sedimentation (45) at 2,000 m. Calculations of NRS and CRS accumulation rates assumed a porosity of 0.5 and average solids density of 2.7 $g{\cdot}cm^{-3}$. The sedimentary record of the narrow GoAq and SRS regions may include a significant terrigenous component.

aragonite is not preserved in deep RS cores (17, 40, 49). It is clear that basin-scale estimates based on water chemistry work on very different spatial and temporal scales than sediment cores, yet the effect of ocean acidification is expected to lower calcification rates. Hence, export production in the past should have been similar to or higher than the current rates. These results strongly support the claim presented by Milliman et al. (50) that 40–80% of the surface-produced $CaCO_3$ dissolves above the chemical lysocline at the upper 800–1,000 m of the ocean. It should, however, be noted that our analyses were not sensitive to high-Mg calcite precipitated by the abundant shallow water echinoderms, which may account for part of the calculated gap between pelagic sedimentation and accumulation rates.

Implication for Evaluating the Effect of Ocean Acidification. Here we established a 1998 baseline for the total $CaCO_3$ precipitation rate in the Red Sea and the relative proportions of coral reefs and calcareous plankton in three oceanic regions, based on a single oceanographic transect. During the 16 y elapsed since these data were collected, the atmospheric pCO_2 rose by more than 30 ppmv (51). The calculated effect of ocean acidification resulting from this rise in atmospheric CO_2 is a decrease in surface water degree of saturation for aragonite, $\Omega_{aragonite}$, of 0.2 and for calcite, $\Omega_{calcite}$, of 0.3. According to the empirical relationship between coral calcification and aragonite saturation developed by Silverman et al. (52), a $\Omega_{aragonite}$ decrease by 0.2 reduces reef calcification rate by 12%, which up to date should have increased the GoAq A_T by 3 $\mu eq \cdot kg^{-1}$. A detailed study on long-term calcification rates of Great Barrier Reef corals found that calcification rates slightly increased from 1900 to 1970 and decreased sharply after 1990 (53). In the RS, a sharp decrease in the calcification rates of single colonies was observed after 1998 (24, 54). If calcification rates of calcareous plankton decreased as well, the increase in normalized alkalinity along the RS should at present be larger than the analytical uncertainty.

This study demonstrates the importance of conducting oceanographic transects similar to that of 1998 in selected basins once every several years to build regional-scale databases for assessing the threat posed by ocean acidification to calcifying organisms. The approach presented here is applicable for open ocean settings and is particularly useful for regions with high calcification rates.

Methods

Sampling. RS and IO surface waters were sampled between October 23 and November 6, 1998, during a cruise of R/V *Sea Surveyor* from Eilat, northern GoAq, to the Seychelles archipelago (Fig. 1). In parallel, water samples from the GoAq and NRS were collected between November 2 and 6, 1998, during a cruise of a chartered vessel, *Queen of Sheba*. The samples on the R/V *Sea Surveyor* were all surface water collected underway every ~100 km using a specially designed water sampler.

Analytical Methods. Salinity was measured using an AGE Minisal 2100 salinometer (internal precision of ±0.003 practical salinity units). Total alkalinity (A_T) was measured by Gran-type titration and calculation (precision of ±1 μeq) after filtering the water samples through 0.45-μm Millipore filter. Na, Ca, Sr, and Mg were analyzed in triplicate by inductively coupled plasma optical emission spectrometry (ICP-OES) on a fully automated Perkin-Elmer Optima-3000 radial ICP system, using the Na589.592, Ca396.847, Sr407.771, and Mg280.270 spectral lines. The samples were filtered through 0.45-μm Millipore filter and diluted with deionized water (18.3 $M\Omega\ cm^{-1}$) to optimal analytical ranges before the measurement. The internal precision of the ICP analysis was typically better than 0.3% (relative standard deviation). Concentrations of blanks were negligible relative to sample concentrations. Much of the analytical instability originated in the sample introduction system; hence the precision of ion ratios was much better than that of the individual ions (55). We corrected this error by normalizing the concentrations of all measured ions to salinity of 35 using the measured Na concentrations. Calibration solutions for ICP runs were prepared from Merck single-element standard solutions. Instrument drift was monitored by running calibration standard sets after every 10-sample batch and was corrected by an off-line, in-house program.

ACKNOWLEDGMENTS. The authors wish to thank the director and staff of the Inter University Institute for Marine Sciences in Eilat for organizing the cruise to Seychelles and Mr. David Hillel, the captain of RV *Sea Surveyor*, and his crew and the crew of *Queen of Sheba*. We thank Tanya Rivlin and Murielle Drey for technical assistance. We thank Adam Subhas for his comments on an earlier version of this manuscript. We acknowledge the Israel Science Foundation for continued support of J.E. and B.L. that enabled this research. We acknowledge the support of the Bill and Melinda Gates Foundation. A scholarship from the Israeli Ministry of Science and Technology was used to support Z.S. during this study.

1. Doney SC, Fabry VJ, Feely RA, Kleypas JA (2009) Ocean acidification: The other CO_2 problem. *Annu Rev Mar Sci* 1:169–192.
2. Orr JC, et al. (2005) Anthropogenic ocean acidification over the twenty-first century and its impact on calcifying organisms. *Nature* 437(7059):681–686.
3. Ries JB, Cohen AL, McCorkle DC (2009) Marine calcifiers exhibit mixed responses to CO_2-induced ocean acidification. *Geology* 37(12):1131–1134.
4. Kroeker KJ, Kordas RL, Crim RN, Singh GG (2010) Meta-analysis reveals negative yet variable effects of ocean acidification on marine organisms. *Ecol Lett* 13(11):1419–1434.
5. Andersson AJ, Gledhill D (2013) Ocean acidification and coral reefs: Effects on breakdown, dissolution, and net ecosystem calcification. *Annu Rev Mar Sci* 5:321–348.
6. Murray SP, Johns W (1997) Direct observations of seasonal exchange through the Bab el Mandab Strait. *Geophys Res Lett* 24(21):2557–2560.
7. Sofianos SS, Johns WE (2002) An Oceanic General Circulation Model (OGCM) investigation of the Red Sea circulation: 1. Exchange between the Red Sea and the Indian Ocean. *J Geophys Res* 107(C11):3196.
8. Sofianos SS, Johns WE (2003) An Oceanic General Circulation Model (OGCM) investigation of the Red Sea circulation: 2. Three-dimensional circulation in the Red Sea. *Journal of Geophysical Research-Oceans* 108(C3):3066.
9. Lazar A (2012) Inertial instability in oceanic flows. PhD thesis (Ecole Polytechnique, Paris).
10. Levy M, et al. (2007) Basin-wide seasonal evolution of the Indian Ocean's phytoplankton blooms. *J Geophys Res* 112(C12):C12014.
11. Poisson A, Morcos S, Souvermezoglou E, Papaud A, Ivanoff A (1984) Some aspects of biogeochemical cycles in the Red Sea with special reference to new observations made in summer 1982. *Deep-Sea Res, Part A* 31(6-8):707–718.
12. Cember RP (1988) On the sources, formation, and circulation of Red Sea deep water. *J Geophys Res* 93(C7):8175–8191.
13. Metzl N, Moore B, Papaud A, Poisson A (1989) Transport and carbon exchanges in Red Sea inverse methodology. *Global Biogeochem Cycles* 3(1):1–26.
14. Krumgalz BS, Erez J (1984) *Chemical Oceanography Survey of the Northern Red Sea, the Straits of Tiran and the Gulf of Elat* (Israel Oceanographic and Limnological Research, Ltd., Haifa, Israel).
15. The Regional Organization for the Conservation of the Environment of the Red Sea & Gulf of Aden (PERSGA) (2010) *The Status of Coral Reefs in the Red Sea and Gulf of Aden: 2009* (PERSGA, Jeddah, Saudi Arabia).
16. Spalding MD, Grenfell AM (1997) New estimates of global and regional coral reef areas. *Coral Reefs* 16(4):225–230.
17. Almogi-Labin A, Hemleben C, Meischner D (1998) Carbonate preservation and climatic changes in the central Red Sea during the last 380 kyr as recorded by pteropods. *Mar Micropaleontol* 33(1-2):87–107.
18. Bouilloux A, et al. (2013) Influence of seawater exchanges across the Bab-el-Mandeb Strait on sedimentation in the Southern Red Sea during the last 60 ka. *Paleoceanography* 28(4):675–687.
19. Dietrich G, Düing W, Grasshoff K, Koske PH (1966) *Physikalische und chemische daten nach beobachtungen des forschungsschiffes "Meteor" im Indischen Ozean 1964 - 65* (Borntraeger, Berlin).
20. Weiss RF, Broecker WS, Craig H, Spencer D (1983) *Hydrographic Data 1977–1978*, GEOSECS Indian Ocean Expedition (US Gov Printing Off, Washington DC), Vol 5.
21. Anderson L, Dyrssen D (1994) Alkalinity and total carbonate in the Arabian Sea. Carbonate depletion in the Red Sea and Persian Gulf. *Mar Chem* 47(3-4):195–202.
22. Craig H (1966) Isotopic composition and origin of the Red Sea and Salton Sea geothermal brines. *Science* 154(3756):1544–1548.
23. Grasshoff K (1969) *Zur chemie des Roten Meeres und des inneren Golfs von Aden nach beobachtungen von F. S. 'Meteor' während der Indischen Ozean expedition 1964/65* (Borntraeger, Berlin).
24. Cantin NE, Cohen AL, Karnauskas KB, Tarrant AM, McCorkle DC (2010) Ocean warming slows coral growth in the central Red Sea. *Science* 329(5989):322–325.
25. Milliman JD (1974) *Marine Carbonates* (Springer, Berlin).
26. Elderfield H, Bertram CJ, Erez J (1996) Biomineralization model for the incorporation of trace elements into foraminiferal calcium carbonate. *Earth Planet Sci Lett* 142(3-4): 409–423.
27. Müller MN, et al. (2014) Influence of temperature and CO_2 on the strontium and magnesium composition of coccolithophore calcite. *Biogeosciences* 11(4):1065–1075.
28. Stoll HM, Schrag DP (2000) Coccolith Sr/Ca as a new indicator of coccolithophorid calcification and growth rate. *Geochem Geophys Geosyst* 1:1999GC000015.
29. Stoll HM, Ziveri P, Shimizu N, Conte M, Theroux S (2007) Relationship between coccolith Sr/Ca ratios and coccolithophore production and export in the Arabian Sea and Sargasso Sea. *Deep Sea Res, Part II* 54(5-7):581–600.

30. Ramaswamy V, Gaye B (2006) Regional variations in the fluxes of foraminifera carbonate, coccolithophorid carbonate and biogenic opal in the northern Indian Ocean. *Deep Sea Res, Part I* 53(2):271–293.
31. Kleijne A, Kroon D, Zevenboom W (1989) Phytoplankton and foraminiferal frequencies in northern Indian Ocean and Red Sea surface waters. *Neth J Sea Res* 24(4):531–539.
32. Correge T (2006) Sea surface temperature and salinity reconstruction from coral geochemical tracers. *Palaeogeogr Palaeoclimatol Palaeoecol* 232(2-4):408–428.
33. de Villiers S (1999) Seawater strontium and Sr/Ca variability in the Atlantic and Pacific oceans. *Earth Planet Sci Lett* 171(4):623–634.
34. Enmar R, et al. (2000) Diagenesis in live corals from the Gulf of Aqaba. I. The effect on paleo-oceanography tracers. *Geochim Cosmochim Acta* 64(18):3123–3132.
35. Broecker WS, Oversby VM (1971) *Chemical Equilibria in the Earth* (McGraw-Hill, New York).
36. Ries JB (2004) Effect of ambient Mg/Ca ratio on Mg fractionation in calcareous marine invertebrates: A record of the oceanic Mg/Ca ratio over the Phanerozoic. *Geology* 32(11):981–984.
37. Segev E, Erez J (2006) Effect of Mg/Ca ratio in seawater on shell composition in shallow benthic foraminifera. *Geochem Geophys Geosyst* 7:Q02P09.
38. Jonkers L, Jimenez-Amat P, Mortyn PG, Brummer GJA (2013) Seasonal Mg/Ca variability of *N. pachyderma* (s) and *G. bulloides*: Implications for seawater temperature reconstruction. *Earth Planet Sci Lett* 376:137–144.
39. Cohen AL, Gaetani A (2010) Ion partitioning and the geochemistry of coral skeletons: solving the mystery of the vital effect. *Ion Partitioning in Ambient-Temperature Aqueous Systems,* EMU Notes in Mineralogy, eds Prieto M, Stoll HM (Eur Mineral Union, London), Vol 10, pp 377–397.
40. Luz B, Heller-Kallai L, Almogi-Labin A (1984) Carbonate mineralogy of late Pleistocene sediments from the northern Red Sea. *Isr J Earth Sci* 33(4):157–166.
41. Danielsson LG, Dyrssen D, Graneli A (1980) Chemical investigations of Atlantis II and Discovery brines in the Red Sea. *Geochim Cosmochim Acta* 44(12):2051–2065.
42. Sen Gupta R, Naqvi SWA (1984) Chemical oceanography of the Indian Ocean, north of the equator. *Deep-Sea Res, Part A* 31(6-8):671–706.
43. Kinsey DW (1985) Metabolism, calcification and carbon production. I. System level studies. *Proceedings of the 5th International Coral Reef Congress* (Antenne Museum, Moorea, French Polynesia), Vol 4, pp 503–542.
44. Takahashi T, et al. (2014) Climatological distributions of pH, pCO_2, total CO_2, alkalinity, and $CaCO_3$ saturation in the global surface ocean, and temporal changes at selected locations. *Mar Chem* 164:95–125.
45. Honjo S, Manganini SJ, Krishfield RA, Francois R (2008) Particulate organic carbon fluxes to the ocean interior and factors controlling the biological pump: A synthesis of global sediment trap programs since 1983. *Prog Oceanogr* 76(3):217–285.
46. Berelson WM, et al. (2007) Relating estimates of $CaCO_3$ production, export, and dissolution in the water column to measurements of $CaCO_3$ rain into sediment traps and dissolution on the sea floor: A revised global carbonate budget. *Global Biogeochem Cycles* 21(1):GB1024.
47. Sabine CL, Key RM, Feely RA, Greeley D (2002) Inorganic carbon in the Indian Ocean: Distribution and dissolution processes. *Global Biogeochem Cycles* 16(4):1067.
48. Froelich PN, et al. (1979) Early oxidation of organic-matter in pelagic sediments of the Eastern Equatorial Atlantic: Suboxic diagenesis. *Geochim Cosmochim Acta* 43(7): 1075–1090.
49. Friedman GM (1965) Occurrence and stability relationships of aragonite, high-magnesian calcite, and low-magnesian calcite under deep-sea conditions. *Geol Soc Am Bull* 76(10):1191–1195.
50. Milliman JD, et al. (1999) Biologically mediated dissolution of calcium carbonate above the chemical lysocline? *Deep Sea Res, Part I* 46(10):1653–1669.
51. National Oceanic and Atmospheric Administration (2014) Mauna Loa CO_2 data. Available at co2now.org/Current-CO2/CO2-Now/noaa-mauna-loa-co2-data.html. Accessed June, 2014.
52. Silverman J, Lazar B, Cao L, Caldeira K, Erez J (2009) Coral reefs may start dissolving when atmospheric CO_2 doubles. *Geophys Res Lett* 36(5):L05606.
53. De'ath G, Lough JM, Fabricius KE (2009) Declining coral calcification on the Great Barrier Reef. *Science* 323(5910):116–119.
54. Arz HW, Lamy F, Pätzold J, Muller PJ, Prins M (2003) Mediterranean moisture source for an early-Holocene humid period in the northern Red Sea. *Science* 300(5616): 118–121.
55. Katz A, Nishri A (2013) Calcium, magnesium and strontium cycling in stratified, hardwater lakes: Lake Kinneret (Sea of Galilee), Israel. *Geochim Cosmochim Acta* 105:372–394.
56. Jameson SC, McManus JW, Spalding MD (1995) State of the Reefs: Regional and Global Perspectives, International Coral Reef Initiative Executive Secretariat Background paper. Available at www.ncdc.noaa.gov/paleo/outreach/coral/sor/index.html. Map available at www.ncdc.noaa.gov/paleo/outreach/coral/sor/images/map2-large.gif. Accessed September 1, 2014.
57. Balch W, Drapeau D, Bowler B, Booth E (2007) Prediction of pelagic calcification rates using satellite measurements. *Deep Sea Res, Part II* 54(5-7):478–495.